HIDDEN MARKOV MODELING FOR MAXIMUM LIKELIHOOD NEURON RECONSTRUCTION

THOMAS L. ATHEY

Center of Imaging Science and Kavli Neuroscience Discovery Institute & Department of Biomedical
Engineering
The Johns Hopkins University

DANIEL TWARD

Department of Computational Medicine & Department of Neurology University of California at Los Angeles

ULRICH MUELLER

Department of Neuroscience The Johns Hopkins University

MICHAEL I. MILLER

Center of Imaging Science and & Department of Biomedical Engineering
The Johns Hopkins University
301 Clark Hall
Baltimore, MD 21218

ABSTRACT. Recent advances in brain clearing and imaging have made it possible to image entire mammalian brains at sub-micron resolution. These images offer the potential to assemble brain-wide atlases of projection neuron morphology, but manual neuron reconstruction remains a bottleneck. Here we present a method inspired by hidden Markov modeling and appearance modeling of fluorescent neuron images that can automatically trace neuronal processes. Our method leverages dynamic programming to scale to terabyte sized image data and can be applied to images with one or more neurons. We applied our algorithm to the output of image segmentation models where false negatives severed neuronal processes, and showed that it can follow axons in the presence of noise or nearby neurons. Our method has the potential to be integrated into a semi or fully automated reconstruction pipeline. Additionally, it creates a framework through which users can intervene with hard constraints to, for example, rule out certain reconstructions, or assign axons to particular cell bodies.

E-mail addresses: tathey1@jhu.edu, DTward@mednet.ucla.edu, umuelle3@jhmi.edu, mim@cis.jhu.edu.

Date: October 20, 2021.

1. Introduction

Recognizing that neuronal processes are one dimensional structures, we use the contour representations from computer vision (see for example [5]) to represent axons, and exploit the computational properties of dynamic programming along absolutely ordered structures. Our probabilistic models are hidden Markov random fields, but we reduce the computational structure to a hidden Markov model (HMM) since the latent structures are absolutely ordered. Hidden Markov modeling involves two sequences of variables, one is observed and one is hidden. A popular application of HMM's is in speech recognition where the observed sequence is an audio signal, and the hidden variables a sequence of words [6]. In our setting, the observed data is the image, and the hidden data is the underlying active contour representation of the axon or dendrite's path. Maximum a posteriori (MAP) estimation of the hidden variables in an HMM can be done with the well-known Viterbi algorithm, an example of dynamic programming [3].

In this work, we apply our hidden Markov modeling framework to the output of image segmentation models. Convolutional neural networks have shown impressive results in image segmentation [7], but it only takes a few false negatives to sever neuronal processes that are often as thin as one micron (Figure 1). Our method can be used to string together connected components in a binary image mask in order to translate an image segmentation to a neuron reconstruction. The data used in this work comes from the MouseLight project at Janelia Research Campus [9].

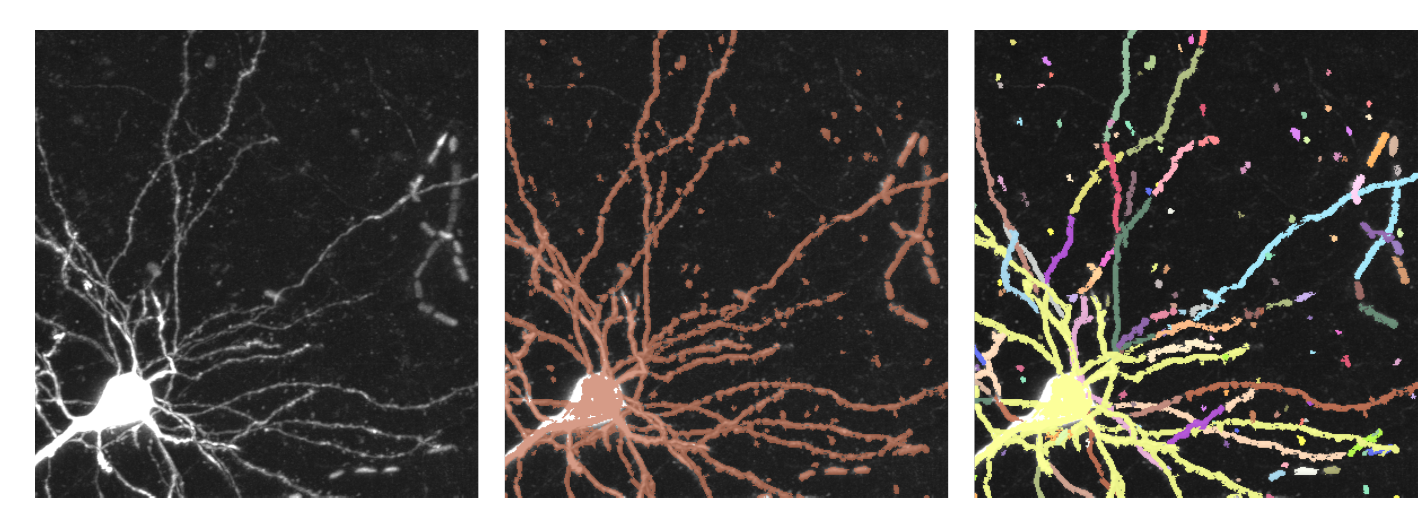


FIGURE 1. Left panel shows an image subvolume from the MouseLight project at Janelia Research Campus containing a single neuron. The middle panel shows the same image overlaid with a binary image mask in brown. This mask was generated by a simple multi-layer perceptron and illustrates the typical output of an image segmentation model. The right panels shows the same binary image mask, with a different color for each connected component. The colors show that the neuron has been severed into several pieces.

2. THE BASIC APPEARANCE IMAGING MODEL

We model the axons as simply connected curves in \mathbb{R}^3 written as a function of arclength

$$c(\ell), \ell \geqslant 0, c(\ell) \in \mathbb{R}^3$$
.

We denote the entire axon curve in space as $c(\cdot) := c(\ell), \ell \ge 0$. To interface the geometric object with the imaging volume we represent the underlying curve as a delta-dirac impulse train in space. We view the

idealized axon model through a point-spread kernel of the imaging platform with point-spread roughly one micron diameter giving our idealized contour representation underlying the measurement process. The point-spread function of the system implies that the axons are well resolved. The fluorescence process given the axon contour $\kappa(\cdot;c)$ is taken as a relatively narrow path through the imaging domain ($\sim 1\mu m$ diameter) with relatively uniform luminance. The imaging model given the contour is taken as a Poisson counting process with intensity $\lambda(y;\kappa),y\in\mathbb{R}^3$ for the flourescence taken as a foreground - backround model:

$$\begin{cases} \lambda(y;\kappa) = \lambda_1, y \in \kappa \\ \lambda(y;\kappa) = \lambda_0, y \notin \kappa \end{cases}.$$

Importantly, we model the image as a conditionally inhomogeneous Poisson process [8] with independent increments given the axon trajectory $\kappa(\cdot)$, the conditioning emphasizes that the underlying latent variable is the axon. In the parlance of computer vision, we can think of the contour model the foreground model, with the complement termed the backround model. Hence the notation λ_1 for the foreground contour, and we will use the notation λ_0 .

2.1. **Fragment Generation as an Intermediate Dimension Reducing Data Structure.** Our fundamental representation of the observed image is as a hidden Markov random field with the axon as the hidden latent structure, exploiting the simplicity of conditional independence conditioned on the axon. Removing the latent position of the axon gives a connected lattice in terms of joint probabilities and neighborhood structures since the foreground and backround intensities must be integrated out as random variables unconditional on the latent axon location.

Given the complexity of sub-micron resolution images, we build an intermediate data structure at the micron scale which we call the fragments $F \in \mathcal{F}$. The fragments themselves are each a collection of lattice sites $F \subset D$. Depicted in Figure 1 the fragments themselves define collections of voxels of varying size |F| that are pieces of the axons without any assumed global ordering. The axons recovery problem becomes the reassembly of the fragments $F \in \mathcal{F}$ along with the imputation of the censored fragments. The complexity of the space of fragments is approximately $|\mathcal{F}| = 100,000$ for a cubic millimeter of projection neuron image data.

The fragments are a coarser scale voxel representation that gives us an efficient data structure upon which we reassemble and can be viewed analogously as higher order features such as edgelets, corners, etc... Reconstructing the ordering of the fragments F_1, F_2, \ldots, F_n as well as the subset of fragments making up the axon becomes equivalent to reconstructing the contour model $\kappa(\cdot)$.

In this work, the first step of fragment generation is classifying each voxel as foreground or background with a neural network. The neural network is trained on binary masks whose foreground is composed of voxels that are sufficiently close to manual neuron traces. During prediction, the probability predictions from the neural network are thresholded at 0.9, a conservative threshold that keeps the number of false positives low.

Next, the connected components of the thresholded image are split into fragments similar size. This is done by identifying the voxel v with the largest predicted foreground probability and placing a ball B_v with radius $5\mu m$ on that voxel. The voxels within B_v are removed and the process is repeated until the component is covered. The component is then split up into pieces by assigning each voxel to the center point v that is closest to it. This procedure ensures that each fragment is no larger than a ball with radius $5\mu m$. At this size, it is reasonable to assume that each fragment is associated with only one axon branch (no fragment is large enough to extensively cover multiple branches).

2.2. Likeliood scoring via Appearance Models of the Observed Images. The imaging process generates the image random field on the voxel lattice $I_{y_i}, i \in \mathcal{Z}_{n^3}$ with a disjoint tiling $D = \bigcup_{i \in \mathcal{Z}^{n^3}} \Delta y_i \subset \mathbb{R}^3$ with each tile center $y_i \in \Delta y_i$. We associate to each lattice voxel center the random field I_{y_i} with mean field of the Poisson process $\int_{\Delta y_i} \lambda(y) dy$. We associate to each lattice site Δy_i the image random field I_{y_i} using the random field notation for any set of sites $Y \subset D$, $I_Y = \{I_{y_i} : \Delta y_i \in Y\}$ is the image random field over Y.

The appearance model associated to the fragment is inhomogeneous Poisson [8] with foreground model conditioned on the fragment:

(1a)
$$\ell(I_F; F) = \prod_{\Delta y_i \in F} \alpha_1(I_{y_i})$$

(1b) with
$$\log \alpha_1(I_{y_i}) = -\int_{\Delta y_i} \lambda_1(y) dy + I_{y_i} \log \int_{\Delta y_i} \lambda_1(y) dy - \log(I_{y_i}!)$$
, $\Delta y_i \in F$.

We notice that in the high light limit we can use the Stirling approximation $\log I_{y_i}! \approx I_{y_i} \log I_{y_i} - I_{y_i}$ giving approximately the logarithm of the foreground modle is negative of the Kullback Liebler distance between the observed image and the foregrand model of luminance:

$$-\log \alpha_1(I_{y_i}) \approx I_{y_i} \log \frac{I_{y_i}}{\int_{\Delta y_i} \lambda_1(y) dy} + (I_{y_i} - \int_{\Delta y_i} \lambda_1(y) dy).$$

The approximation is $O(\log I)$. Notice the second term is centered around 0 on the average since the integral of intensity is the mean of the Poisson random variable (but also its variance).

3. MARKOV STATE REPRESENTATION AND MAP ESTIMATION

We exploit now the computational structures of hidden Markov models when the underlying latent structure is absolutely ordered so that dynamic programming can be used to generate efficient algorithm for maximum a-posteriori estimation. Our conditional or hidden markov process that we build for representing the axon is equivalent to solving the orderining of a sub-sequence of the fragments $f_{1:n} \in \mathcal{F}^n$ by associating to each fragment its startpoint and endpoint $x^0 \in \mathbb{R}^3$, $x^1 \in \mathbb{R}^3$, along with tangent associated to the endpoints $\tau^0 \in \mathbb{R}^3$, $\tau^1 \in \mathbb{R}^3$ (Figure 2). It is useful to define $x(f) = (x^0, x^1)$ with $\tau(f) = (\tau^0, \tau^1)$ which forms the state process:

$$s = (x^0, x^1, \tau^0, \tau^1)$$
.

Our computational algorithms exploit two splitting properties, the Markov nature of the states and the splitting of the random field image given the state sequence. We use the notation $s_{i:j} := (s_i, s_{i+1}, \dots, s_j)$. We model the state sequence s_1, \dots, s_n as Markov with splitting property:

$$p(s_{k+1:n}, s_{1:k-1}|s_k) = p(s_{k+1:n}|s_k)p(s_{1:k-1}|s_k), k = 2, \dots, n-1,$$

which implies the 1-order Markov property $p(s_i|s_{i-1},s_{1:i-2})=p(s_i|s_{i-1}), i=1,\ldots,n$ with $p(s_1|s_0)=\pi(s_1)$ the initial distribution. To construct the Markov chain we use tilted Gaussian models, normalized over the discrete state space:

$$p(s_i|s_{i-1}) = \frac{e^{-\alpha|x_i^0 - x_{i-1}^1|^2}}{Z(s_{i-1})},$$

with the normalizer given by $Z(s_{i-1}) = \sum_{s_i \in \mathcal{S}} e^{-\alpha |x_i^0 - x_{i-1}^1|^2}$. We choose $1/\alpha = 2\sigma^2$ with $1\mu < \sigma < 3\mu$.

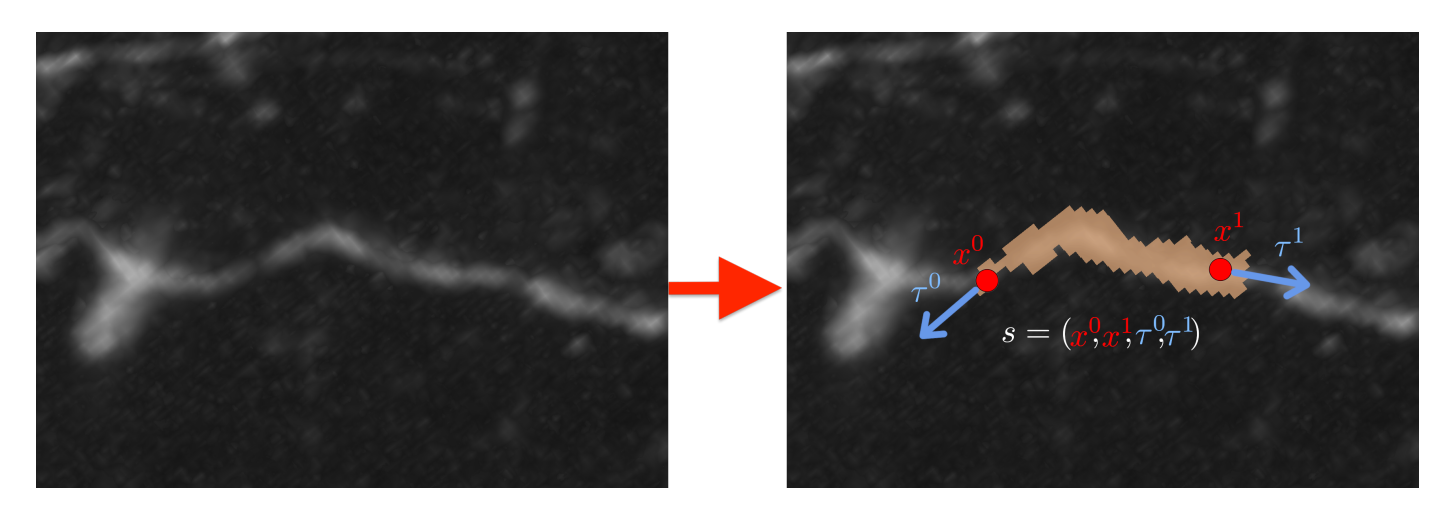


FIGURE 2. Left panel is an image subvolume containing part of a neuronal process. Right panel is the same image overlaid with a light brown mask depicting one of the fragments. From the fragment we estimate the endpoints (red points), and the tangents at the endpoints (blue arrows).

3.1. Conditionally independent observable image model given the state process. The state sequence determines the set of sites which are the foreground associated to neuron location. We denote the locations of the axon fragments as $x(s) = ((x^0, x^1)(s))$, with the sequence of fragment endpoint pairs determined by the state sequence $x(s_{1:n}) = ((x^0, x^1)(s_1), \dots, (x^0, x^1)(s_n))$.

The observables are the image random field, taken as conditionally independent increments given the state:

$$p(I_{x(s_i)}, I_{D\setminus x(s_i)}|s_i,) = p(I_{x(s_i)}|s_i)p(I_{D\setminus x(s_i)}|s_i)$$
,

which implies $p(I_{x(s_i)}|s_i, I_{D\setminus x(s_i)}) = p(I_{x(s_i)}|s_i)$.

Define the maximizer of the posterior probability (MAP) on the state sequence $s_{1:n} \in \mathcal{S}^n$, with $|\mathcal{S}|$ finite:

(2)
$$\hat{s}_{1:n} := \operatorname{argmax}_{s_{1:n} \in \mathcal{S}^n} \log p(s_{1:n}|I_D).$$

To generate a global maximizer we would have to evaluate over $|S|^n$ sequences which is not possible. We rewrite the MAP estimator in terms of the joint probability allowing us to write the recursion:

$$\hat{s}_{1:n} = \operatorname{argmax}_{s_{1:n} \in \mathcal{S}^n} p(s_{1:n} | I_D) = \operatorname{argmax}_{s_{1:n} \in \mathcal{S}^n} p(s_{1:n}, I_{x_{1:n}}, I_{D \setminus x_{1:n}}).$$

We use these splitting properties to define the recursive calculation for calculating the maximum a-posteriori sequences. We define the indicator function $\delta_A(x) = 1$ for $x \in A$, 0 otherwise.

Lemma 1. Then for n > 1 we have

(3)
$$p(s_{1:n}, I_{x_{1:n}}, I_{D \setminus x_{1:n}}) = \left(\frac{\alpha_1(I_{x_n})}{\alpha_0(I_{x_n})}\right)^{\delta_{D \setminus x_{1:n-1}}(x_n)} p(s_n | s_{n-1}) p(s_{1:n-1}, I_{x_{1:n-1}}, I_{D \setminus x_{1:n-1}}),$$

Proof.

$$p(s_{1:n}, I_{x_{1:n}}, I_{D \setminus x_{1:n}}) = p(I_{x_n} | s_{1:n}, I_{x_{1:n-1}}, I_{D \setminus x_{1:n}}) p(s_n | s_{1:n-1}, I_{D \setminus x_{1:n}}) p(s_{1:n-1}, I_{x_{1:n-1}}, I_{D \setminus x_{1:n}})$$

$$= p(I_{x_n} | s_n)^{\delta_{D \setminus x_{1:n-1}}(x_n)} p(s_n | s_{n-1}) p(s_{1:n-1}, I_{x_{1:n-1}}, I_{D \setminus x_{1:n}})$$

$$= \alpha_1(I_{x_n})^{\delta_{D \setminus x_{1:n-1}}(x_n)} p(s_n | s_{n-1}) p(s_{1:n-1}, I_{x_{1:n-1}}, I_{D \setminus x_{1:n}})$$

$$(4)$$

We rewrite the last term using the splitting property:

$$\begin{split} p(s_{1:n-1},I_{x_{1:n-1}},I_{D\backslash x_{1:n}}) &= p(I_{x_{1:n-1}}|s_{1:n-1},I_{D\backslash x_{1:n}})p(s_{1:n-1},I_{D\backslash x_{1:n}}) \\ &= p(I_{x_{1:n-1}}|s_{1:n-1})p(I_{D\backslash x_{1:n}}|s_{1:n-1})p(s_{1:n-1}) \\ &= p(I_{x_{1:n-1}}|s_{1:n-1})\frac{p(I_{D\backslash x_{1:n-1}}|s_{1:n-1})}{p(I_{x_n}|s_{1:n-1})^{\delta_{D\backslash x_{1:n-1}}(x_n)}}p(s_{1:n-1}) \\ &= \frac{1}{\alpha_0(I_{x_n})^{\delta_{D\backslash x_{1:n-1}}(x_n)}}p(s_{1:n-1},I_{x_{1:n-1}},I_{D\backslash x_{1:n-1}}) \end{split}$$

with the last substitution following from the definition of the background model. Substituting into (4) yields:

(5)
$$p(s_{1:n}, I_{x_{1:n}}, I_{D\setminus x_{1:n}}) = \left(\frac{\alpha_1(I_{x_n})}{\alpha_0(I_{x_n})}\right)^{\delta_{D\setminus x_{1:n-1}}(x_n)} p(s_n|s_{n-1})p(s_{1:n-1}, I_{x_{1:n-1}}, I_{x_{D\setminus x_{1:n-1}}}).$$

We notice that the puncturing of the domain according to is akin to the factorization in [4] for road tracking.

3.2. Viterbi Algorithm Does Not Apply to This Posterior. Following Forney, we factor $p(s_{1:n}, I_{x_{1:n}}, I_{D\setminus x_{1:n}})$ by repeatedly applying 3:

(6)
$$p(s_{1:n}, I_{x_{1:n}}, I_{D \setminus x_{1:n}}) = \prod_{k=1}^{n} \left(\frac{\alpha_1(I_{x_k})}{\alpha_0(I_{x_k})}\right)^{\delta_{D \setminus x_{1:k-1}}(x_k)} p(s_k | s_{k-1})$$

then by taking the negative logarithm:

(7)
$$-\ln p(s_{1:n}, I_{x_{1:n}}, I_{D \setminus x_{1:n}}) = \sum_{k=1}^{n} -\delta_{D \setminus x_{1:k-1}}(x_k) \ln \frac{\alpha_1(I_{x_k})}{\alpha_0(I_{x_k})} - \ln p(s_k | s_{k-1})$$

with $p(s_1|s_0) = \pi(s_1)$ the initial distribution over the states.

In (7), the k'th term in the sum, which corresponds to the cost incurred by the transition from s_{k-1} to s_k , depends on the partial sequence $x_{1:k-1}$. In particular, the cost depends on whether state s_k was already visited. In classic hidden Markov modeling, the k'th term in the sum depends only on the k'th transition, $x_{k-1:k}$. This difference is crucial when it comes to maximizing 6 (or minimizing 7). In our setting, the negative log of the probability or, in statistical mechanics language, the "energy," is not sequentially additive, and the Viterbi algorithm is no longer valid.

Here is a simple counter example demonstrating that the Viterbi algorithm fails to identify the globally optimal state sequence in our setting:

$$S = \{1, 2\}, n = 4, \pi(s_1 = 1) = 1$$
$$\frac{\alpha_1(I_1)}{\alpha_0(I_1)} = 1$$
$$\frac{\alpha_1(I_2)}{\alpha_0(I_2)} = 1/100$$

The transition probabilities are given in Figure 3.

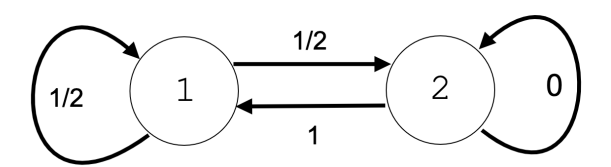


FIGURE 3. Transition probabilities of a two state Markov model that demonstrates the Viterbi algorithm is invalid in our setting.

After three iterations, the Viterbi algorithm stores (1,1,1,2) as the highest probability path of length 4 that ends in state 2 (Figure 4a). The joint probability of this path is 1/800. However, there is an alternative path that the algorithm missed, (1,2,1,2), which has higher joint probability 1/400 (Figure 4b). The algorithm did not identify the globally optimal sequence because it did not "see" that the cost of transitioning from state 1 to 2 would drop from 1/200 to 1/2 after visiting state 2 the first time.

We have now established that the Viterbi algorithm is not guaranteed to find the globally optimal state sequence in our setting, because of a higher order dependence on previous states. However, in the case of a non-repeating state sequence, our joint probability in 6 simplifies to:

(8)
$$p(s_{1:n}, I_{x_{1:n}}, I_{D \setminus x_{1:n}}) = \prod_{k=1}^{n} \frac{\alpha_1(I_{x_k})}{\alpha_0(I_{x_k})} p(s_k | s_{k-1})$$

and

(9)
$$-\ln p(s_{1:n}, I_{x_{1:n}}, I_{D\setminus x_{1:n}}) = \sum_{k=1}^{n} -\ln \frac{\alpha_1(I_{x_k})}{\alpha_0(I_{x_k})} - \ln p(s_k|s_{k-1})$$

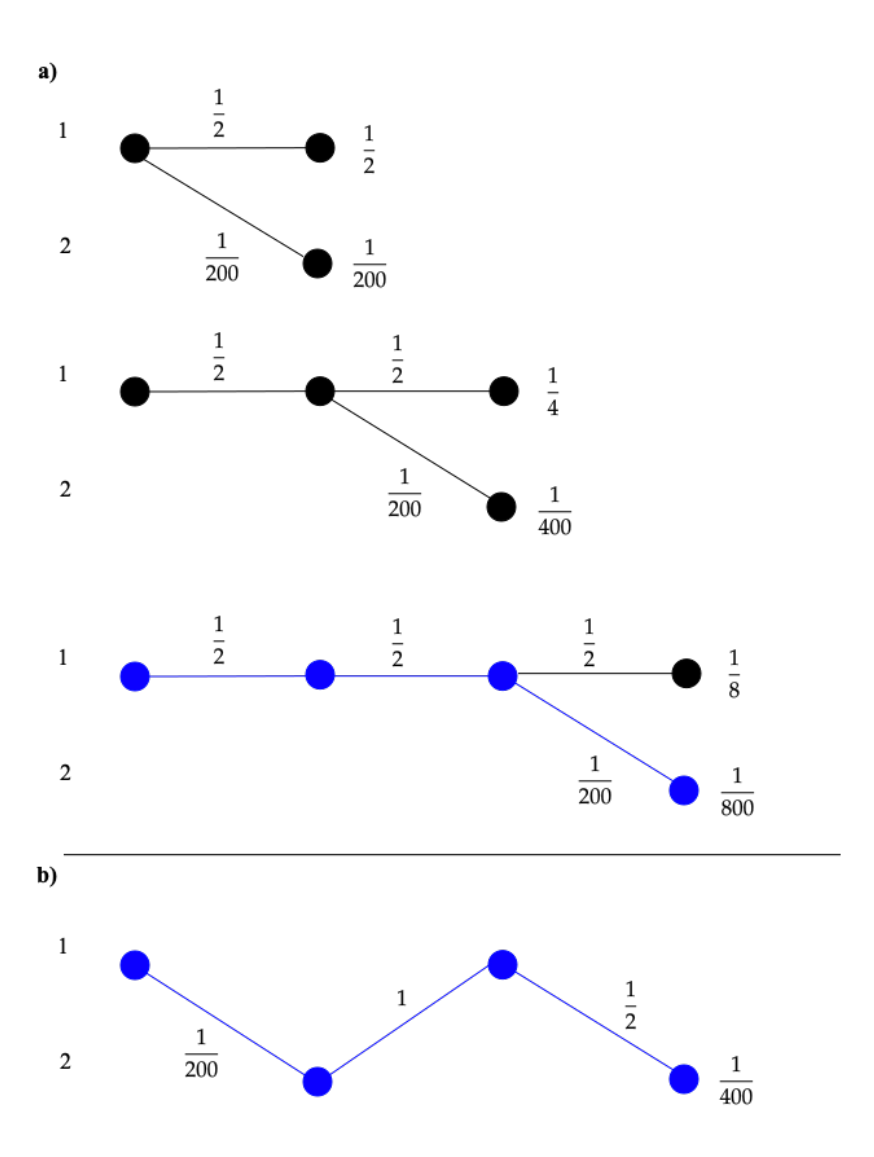
In this case, the cost incurred by the transition from s_{k-1} to s_k is invariant to previous states in the sequence. This invariance is crucial for the Viterbi algorithm to work. We emphasize that 9 only applies to non-repeating sequences, but the following result describes how it may be applicable even in the presence sequences with repeating states.

Proposition 1. Suppose the MAP estimate $s_{1:n}^* = \operatorname{argmax}_{s_{1:n} \in \mathcal{S}^n} p(s_{1:n}|I_D)$ is a non-repeating sequence of states. Further, suppose that $\frac{\alpha_1(I_x)}{\alpha_0(I_x)} \leq 1$ for all x. Then, the Viterbi algorithm applied to 9 is valid, meaning it will return $s_{1:n}^*$.

Proof. For each state s_k that is repeated in the sequence $s_{1:n}$, the right side of Equation 9 has an extra factor of $-\ln\frac{\alpha_1(I_{x_k})}{\alpha_0(I_{x_k})}$. Further, since $\frac{\alpha_1(I_x)}{\alpha_0(I_x)} \leqslant 1$ we have $-\ln\frac{\alpha_1(I_x)}{\alpha_0(I_x)} \geqslant 0$ which shows that the right side of 9 overestimates the true energy $-\ln p(s_{1:n},I_{x_{1:n}},I_{D\setminus x_{1:n}})$. Thus, for all state sequences $s_{1:n}$:

$$-\ln p(s_{1:n}, I_{x_{1:n}}, I_{D\setminus x_{1:n}}) \leqslant \sum_{k=2}^{n} -\ln \frac{\alpha_1(I_{x_k})}{\alpha_0(I_{x_k})} - \ln p(s_k|s_{k-1})$$

FIGURE 4. Example showing that the Viterbi algorithm is invalid in our setting. The nodes represent the states and the line segments represent state transitions, as in Figure 8 of [3]. Panel a) illustrates three iterations of the Viterbi algorithm, with the lines representing the paths that are stored at each iteration. In this example, the blue path at the bottom of panel a) is identified by naive application of the Viterbi algorithm, but it is not the highest probability path of length 4 that ends in state 2 - the shortest such path is shown in panel b). Each transition has a number above it indicating its contribution to the joint probability - $\left(\frac{\alpha_1(I_{x_k})}{\alpha_0(I_{x_k})}\right)^{\delta_{D\setminus x_1:k-1}(x_k)} p(s_k|s_{k-1})$ from Equation 6. The number at the end of the path is the product of all such terms - the joint probability of the given path.



with equality when $s_{1:n}$ is non-repeating. Since $s_{1:n}^*$ minimizes $-\ln p(s_{1:n}, I_{x_{1:n}}, I_{D\setminus x_{1:n}})$, and is non-repeating, it will also minimize this overestimate. Thus the Viterbi algorithm will correctly return the MAP estimate, $s_{1:n}^*$.

4. Overcoming Negative Cycles with Maximum Likelihood Estimation

Unfortunately, in practice, we have $\frac{\alpha_1(I_x)}{\alpha_0(I_x)} > 1$ for states that correspond to where the neuron is very bright. This can lead to negative cycles through the graph of states, making the shortest path problem ill-posed. So, we modify our optimization problem in a way that removes negative cycles and makes it possible to apply shortest-path algorithms Bellman-Ford or Dijkstra's [1, 2]. To avoid negative cycles we move away from a "global probability" calculation removing the complement of the space in the calculation. This removes the denominator in $\frac{\alpha_1(I_x)}{\alpha_0(I_x)}$.

Theorem 1. Define the most-likely solution $s_{1:n} \in \mathcal{S}^n$ by the joint probability

(10)
$$\max_{s_{1:n} \in \mathcal{S}^n} p(s_{1:n}, I_{x_{1:n}}).$$

Then we have

(11)
$$\max_{s_{1:n} \in \mathcal{S}^n} p(s_{1:n}, I_{x_{1:n}}) = \max_{s_{1:n} \in \mathcal{S}^n} \prod_{i=1}^n \left(\alpha_1(I_{x_i})\right)^{\delta_{D \setminus x_{1:i-1}}(x_i)} p(s_i | s_{i-1}),$$

or, written with negative logarithms,

(12)
$$\min_{s_{1:n} \in \mathcal{S}^n} -\ln p(s_{1:n}, I_{x_{1:n}}) = \max_{s_{1:n} \in \mathcal{S}^n} \sum_{i=1}^n -\delta_{D \setminus x_{1:i-1}}(x_i) \ln \alpha_1(I_{x_i}) - \ln p(s_i | s_{i-1}),$$

with
$$p(s_1|s_0) := \pi(s_1), x_{1:0} = \emptyset$$
.

Proof.

$$p(s_{1:n}, I_{x_{1:n}}) = p(s_{1:n}, I_{x_{1:n-1}}, I_{x_n})$$

$$= p(I_{x_n}|s_{1:n}, I_{x_{1:n-1}})p(s_{1:n}, I_{x_{1:n-1}})$$

$$= p(I_{x_n}|s_{1:n}, I_{x_{1:n-1}})p(I_{x_{1:n-1}}|s_{1:n})p(s_{1:n})$$

$$= p(I_{x_n}|s_{1:n}, I_{x_{1:n-1}})p(I_{x_{1:n-1}}|s_{1:n-1})p(s_n|s_{1:n-1})p(s_{1:n-1})$$

$$= (\alpha_1(I_{x_n}))^{\delta_{D\backslash x_{1:n-1}}(x_n)}p(s_n|s_{n-1})p(I_{x_{1:n-1}}|s_{1:n-1})p(s_{1:n-1}).$$

Applying this to factor the conditional probability , $I_{x_{1:i}}, i=n-1,\ldots,1$ gives the joint product. \Box

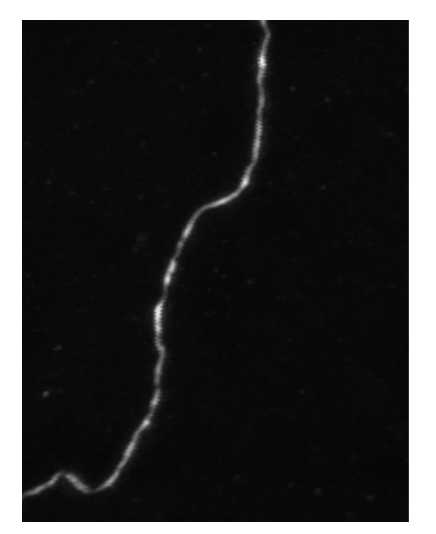
Note that since $\alpha_1(I_{x_i})$ and $p(s_i|s_{i-1})$ are discrete probability distributions, they are bounded by 1 which makes every term in the sum on the right side of 12 non-negative, meaning there are no longer negative cycles in the graph of states.

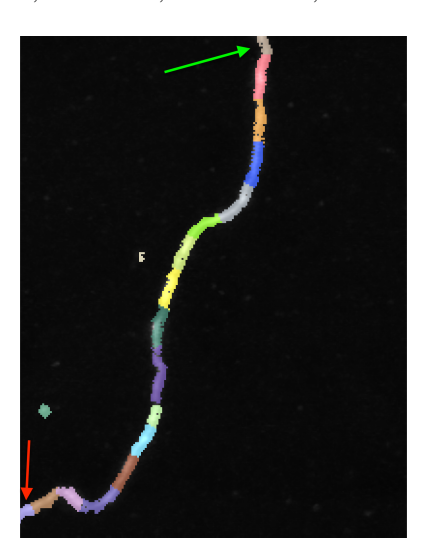
5. APPLICATIONS TO FIXED START AND END STATES

We will focus on the application of our model to cases where the start and end states are fixed. Fixing the start point involves setting the initial distribution $\pi(\cdot)$ to a delta dirac on a particular state. Fixing the end point to a state s_e is less straightforward since it is not obvious when that end point can be reached in the state trellis. Our solution is to modify the transition distribution of that state $p(\cdot|s_e)$ to be a delta dirac located on s_e . Also, we set the length of the sequence, n, sufficiently large so the sequence is forced to go to the end state and remain there (since the cost of all other transitions is positive). This procedure can be extended to several end states, and the state sequence will terminate in one of those several end states.

Now we can reconsider Proposition 1 in this setting, with fixed start and end states. The condition requiring $\frac{\alpha_1(I_x)}{\alpha_0(I_x)} \le 1$ for all x now becomes $\alpha_1(I_x) \le 1$ for all x which is trivially satisfied since α_1 is a discrete probability distribution. Further, since the cost of a transition between two different states is always positive, removing cycles in a state sequence will lower its overall cost. Thus, the maximum likelihood estimate in this setting is a non-repeating sequence of states. Altogether, the idea of Proposition 1 holds in this case, meaning we can apply shortest path algorithms (such as the Viterbi algorithm) to identify globally optimal state sequences.

We demonstrate this procedure first on part of a neuronal process with a fixed start state and a single fixed end state in Figure 5. We also demonstrate this procedure on an axon with a fixed start state and three fixed end states located at three different cell bodies in Figure 6.





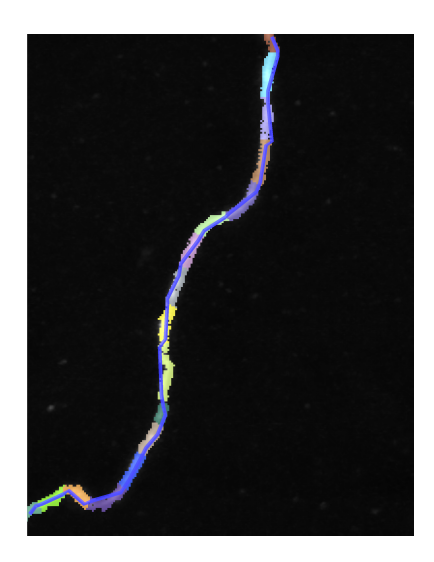
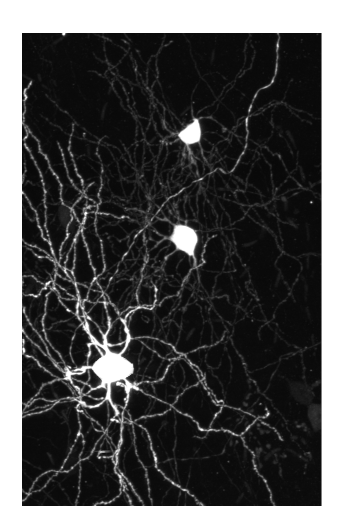
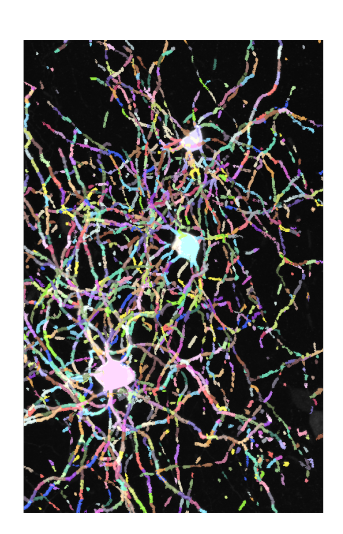
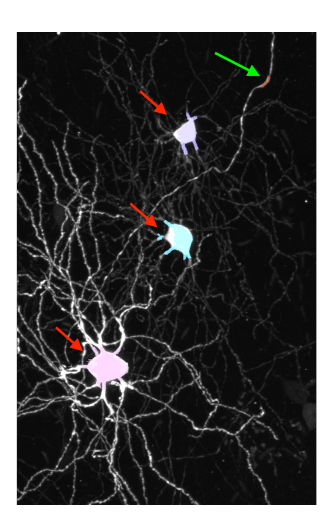


FIGURE 5. Demonstration of our algorithm on part of a neuronal process where the start and end states are fixed. Left panel shows an image subvolume containing a part of an axon. Middle panel shows the same image overlaid with the fragments where each fragment has a unique color. The green arrow indicates the starting fragment and the red arrow indicates the ending fragment. Right panel shows the path selected by the algorithm. The fragments in the path are shown in unique colors and blue line shows the path that connects the endpoints of the fragments.







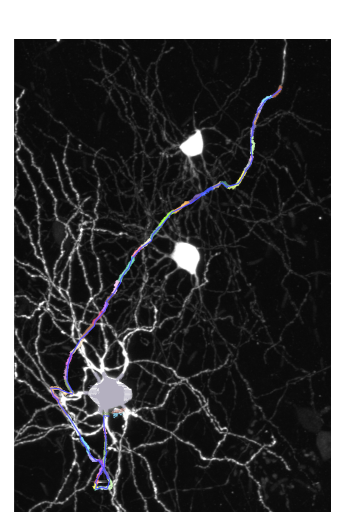


FIGURE 6. Demonstration of our algorithm on part of a neuronal process where the start state is fixed and the end state is one of three somas. Left panel shows an image subvolume containing three somas and many neuronal processes. Second panel shows the same image overlaid with the fragments where each fragment has a unique color. Third panel highlights the fixed start state (green arrow) and the three soma states (red arrows). Right panel shows the path selected by the algorithm. The fragments in the path are shown in unique colors and blue line shows the path that connects the endpoints of the fragments.

6. DISCUSSION

In this work we present a method inspired by hidden Markov modeling that can reconstruct neuronal processes that had been severed in binary image masks. This process involves converting the connected components of an image mask into a set of "fragments" that are no longer than $10\mu m$. From these fragments we estimate the end points, and the orientation of the fragment at those endpoints in order to construct a simplified state space. We demonstrate that estimating sequences in this state space is not possible when conditioning on the entire image due to negative cycles in the graph of states. So, we modify our procedure to a maximum likelihood approach, and it becomes possible to apply shortest path algorithms such as the Viterbi algorithm.

Just like in classic hidden Markov modeling, it is possible leave start and end states fixed or unfixed. We apply the algorithm in the case of fixed start and end points on two-photon image data of neurons in mice. We propose that this method can be used in semi-automatic neuron reconstruction where a tracer could click on two different fragments along a neuronal process, and this algorithm would fill in the gap. Or, this algorithm could be used in a completely automated neuron reconstruction pipeline. The biggest hurdle in extending this algorithm to fully-automated setting would be designing the distributions in the model so they accurately model the underlying neuron generation process. Our future work will be focused on this endeavor, ensuring that the state transition distribution and image emission distribution lead to robust reconstruction of neuronal processes.

APPENDIX A. VITERBI ALGORITHM EXPLOITING THE NON-CYCLIC ASSUMPTION

Examine the viterbi algorithm when there are no cycles, and the cost function is sequentially additive, then for n > 1 we have

(13)
$$p(s_{1:n}, I_{x_{1:n}}, I_{D \setminus x_{1:n}}) = \frac{\alpha_1(I_{x_n})}{\alpha_0(I_{x_n})} p(s_n | s_{n-1}) p(s_{1:n-1}, I_{x_{1:n-1}}, I_{D \setminus x_{1:n-1}}),$$

The maximizers of (13) are given by the following recursion:

(14a)
$$\max_{s_{1:n} \in \mathcal{S}^n} p(s_{1:n}, I_{x_{1:n}}, I_{D \setminus x_{1:n}}) = \max_{s_n \in \mathcal{S}} \rho_n(s_n)$$

(14a)
$$\max_{s_{1:n} \in \mathcal{S}^n} p(s_{1:n}, I_{x_{1:n}}, I_{D \setminus x_{1:n}}) = \max_{s_n \in \mathcal{S}} \rho_n(s_n)$$
(14b)
$$\text{with } \begin{cases} \rho_n(s_n) = \max_{s_{n-1} \in \mathcal{S}} \frac{\alpha_1(I_{x_n})}{\alpha_0(I_{x_n})} p(s_n|s_{n-1}) \rho_{n-1}(s_{n-1}) \\ \rho_1(s_1) = \frac{\alpha_1(I_{x_1})}{\alpha_0(I_{x_1})} p(s_1|s_0) \end{cases}$$

with $p(s_1|s_0) = \pi(s_1)$ the initial distribution on state and $\rho_0 = 1$.

To start the recursion we need $\rho_1(s_1) = p(s_1, I_{x_1}, I_{D \setminus x_{1:1}}) = \frac{\alpha_1(I_{x_1})}{\alpha_0(I_{x_1})} \pi(s_1) \rho_0(s_0)$ where $\pi_{S_1}(\cdot)$ is the initial law on the Markov chain (start state) is the soma with $\rho_0 = 1$.

APPENDIX B. CONFLICT OF INTEREST STATEMENT

MM own Anatomy Works with the arrangement being managed by Johns Hopkins University in accordance with its conflict of interest policies. The remaining authors declare that the research was conducted in the absence of any commercial or financial relationships that could be construed as a potential conflict of interest.

The funders had no role in study design, data collection and analysis, decision to publish, or preparation of the manuscript.

APPENDIX C. FUNDING

This work is supported by the National Institutes of Health grants RF1MH121539

REFERENCES

- [1] Richard Bellman. On a routing problem. Quarterly of applied mathematics, 16(1):87–90, 1958.
- [2] Edsger W Dijkstra. A note on two problems in connexion with graphs. Numerische mathematik, 1(1):269–271, 1959.
- [3] G David Forney. The viterbi algorithm. Proceedings of the IEEE, 61(3):268–278, 1973.
- [4] Donald Geman and Bruno Jedynak. An active testing model for tracking roads in satellite images. *IEEE Transactions on Pattern Analysis and Machine Intelligence*, 18(1):1–14, 1996.
- [5] Michael Kass, Andrew Witkin, and Demetri Terzopoulos. Snakes: Active contour models. *International journal of computer vision*, 1(4):321–331, 1988.
- [6] Lawrence Rabiner and Biinghwang Juang. An introduction to hidden markov models. ieee assp magazine, 3(1):4–16, 1986.
- [7] Olaf Ronneberger, Philipp Fischer, and Thomas Brox. U-net: Convolutional networks for biomedical image segmentation. In *International Conference on Medical image computing and computer-assisted intervention*, pages 234–241. Springer, 2015.
- [8] Donald L Snyder and Michael I Miller. Random point processes in time and space. Springer Science & Business Media, 2012.
- [9] Johan Winnubst, Erhan Bas, Tiago A Ferreira, Zhuhao Wu, Michael N Economo, Patrick Edson, Ben J Arthur, Christopher Bruns, Konrad Rokicki, David Schauder, et al. Reconstruction of 1,000 projection neurons reveals new cell types and organization of long-range connectivity in the mouse brain. *Cell*, 179(1):268–281, 2019.